Deformation of liquid-liquid interfaces by a rotating rod

C. Zhao, C. Gentric, N. Dietrich, Y.G. Ma, Huai-Zhi Li

Deformation of liquid-liquid interfaces by a rotating rod

C.W. Zhao[a], C. Gentric[a], N. Dietrich[a], Y.G. Ma[b] and Huai Z. Li[a*]

[a] Laboratory of Reactions and Process Engineering, CNRS, University of Lorraine

1 rue Grandville, BP 20451, 54001 Nancy Cedex, France

[b] State Key Laboratory of Chemical Engineering, School of Chemical Engineering and Technology, Tianjin University, Tianjin 300072, China

* corresponding author: Huai-Zhi.Li@univ-lorraine.fr

The present study aims at investigating the deformation mechanism of liquid-liquid interfaces by both the experimental and numerical approaches. The experiments reveal that the topology of an initial flat interface composed of a Newtonian aqueous and a Newtonian oil phases can be modulated as climbing or descending along a rotating rod according to the ratio of the kinematic viscosity between these two liquid phases. The measurements of the fluid flow fields by PIV highlight the relationship between the appearance of the Taylor-Couette instability in the less viscous phase and the interface's orientation. The increasing rod rotation speed expands the Taylor-Couette vortices, and intensifies then the magnitude of the interface deformation. The numerical simulation by the VOF method is in qualitative agreement with the experimental results, in particular the interface shape and the qualitative influence of different parameters, even under very high rotation speeds of the rod.

Keywords: dynamical deformation, liquid-liquid interface, rod climbing, Newtonian fluid,

PIV measurement, VOF simulation

I. INTRODUCTION

Fluid-fluid interfaces are widely encountered in both academic research and industrial applications[1]. In particular, the mobile and deformable characteristics of liquid-liquid interfaces are essential for the understanding of a variety of natural and industrial processes, such as cell behavior, drop coalescence, emulsification processes, liquid–liquid extraction, interfacial mass transfer and chemical reactions[2-4].

Some works in the literature have been devoted to the breakthrough problem of liquid-liquid interfaces between two immiscible liquids due to the passage of particles. Most of them consider the approach of a solid sphere[5,6] or a liquid drop[7,8] towards a deformable interface with a focus on the film drainage and coalescence. The study of a rising gas bubble through a liquid-liquid interface concerns generally the behavior of the interface before and after the passage of the bubble such as the drift volume[9,10]. Recently, the flow fields close to the deforming interface were experimentally investigated by Particle Image Velocimetry technique (PIV)[6,8,9,10]. On the numerical side, there are still relatively few works performed for the deformation of the liquid-liquid interface. Bonhomme *et al*.[9] employed a volume of fluid approach to compare with the experimental dynamics of an isolated bubble crossing through a horizontal fluid-fluid interface. Geller *et al*.[11] simulated the approach of a rigid

sphere normal to a deformable liquid-liquid interface under the creeping motion condition to neglect inertial effects.

Following these previous works, a new possibility is to deform liquid-liquid interfaces by making use of a rotating rod instead of moving particles. The main advantage of a rotating rod for a given rotation speed is to impose a constant stimulus and then to avoid the transient phenomenon accompanying the passage of a particle towards the interface. A complementary motivation stems from a strange phenomenon[12] experimentally observed when a rotating rod was immersed into a beaker with two immiscible Newtonian fluids: the liquid-liquid interface can surprisingly climb the rod like the well-known Weissenberg effect in viscoelastic fluids[13]. If the preliminary experimental results tended to show a possible origin of hydrodynamic instability, further experimental and numerical works are still required to understand better this rod climbing behavior phenomenon.

The present works aims then at studying the dynamical behavior of liquid–liquid interfaces under a controlled stimulus, in particular the deformation of an immiscible liquid-liquid interface formed by a heavy and a light Newtonian liquids with different rods under various rotation speeds. Extensive experiments were performed in order to get a better understanding of the topological modulation of the liquid-liquid interface composed of various Newtonian liquids, including of course the rod-climbing effects. Besides the fundamental mechanisms, the circumstance of a spinning cylinder in an interface may find widespread applications such as the mixing between two liquid phases by a mechanical stirrer in a tank, or more precisely

the emulsification process through a high-shearing rotor-stator device in which the rotation of the rotor deforms and breaks up the interface to produce droplets dispersed in another liquid. The experimental setup was voluntarily chosen to be quite different from a classical Taylor-Couette device[14]. In fact, a very large column filled with two different Newtonian fluids was employed to avoid the spatially confined flow, in particular with a relatively small rotating rod similar to an experiment for the Weissenberg effect in viscoelastic fluids. It is worth mentioning that Taylor-Couette flows take place usually in a single component liquid phase within a narrow gap between two confined concentric cylinders. The Volume Of Fluid (VOF) was also applied to simulate the complex flow features and to compare with the experimental results. To some extent, this work is the natural extension of our previous studies on the dynamical deformation of a flat liquid-liquid interface by the sedimentation of a solid sphere[6] or the ascension of a gas bubble[10]. From the point view of industrial applications, it is also more flexible to varying various stimuli by different rod nature (hydrophobic or hydrophilic), rod diameter, and rotation speed as well as liquid-liquid couple. These parameters are frequently encountered in an industrial emulsification process[15].

II. EXPERIMENTAL SETUP

The experimental setup consisted of a square column in glass of 11 cm width and 16 cm height to facilitate the measurements of the flow fields and the visualization. Two immiscible Newtonian fluids were used to form a liquid-liquid interface: an organic phase with silicon oil (SO) of different viscosity: 11, 111, 500 and 1000 mPa.s as light liquid and an aqueous phase

with Emkarox (HV45) solutions of various mass concentrations: 0%, 25%, 50% and 65% as heavy liquid. A Rheometric Fluid Spectrometer RFS II (TA Instruments, USA) was employed to measure the viscosity of these liquids. The interfacial tension between the various couples silicon oil/aqueous solution was measured using a Tracker tensiometer (I.T. Concept, France). The properties of these liquids used are summarized in Table I and Table II respectively. All experiments were carried out at constant temperature of 293K.

An initial flat liquid-liquid interface was very carefully realized by filling the column firstly with the aqueous phase, then with the organic light phase. The introduction of the latter phase over the first one was smoothly and progressively to avoid any disturbance at the interface. Before the filling, the glass column was cleaned up by liquid detergents to minimize the meniscus at the wall so that the visualization was facilitated. The immersed rotating rods were composed of three materials including stainless steel, polyvinyl chloride (PVC) and polytetrafluoroethylene (Teflon) and had three different diameters: d = 6, 8 and 10 mm respectively. No measurable difference was observed between three materials of rods. In fact, the contact angle at the contact line between the liquid-liquid interface and the rod seems to be close to 90° whatever the rod's nature from the images under the static conditions without rotation. Of course, the presence of a meniscus near the column wall in front of the camera did not allow to experimentally distinguishing with accuracy the difference of the contact angle between the various rods. This tends to show that the Weissenberg-like effect is mainly governed by the hydrodynamics, not by the wetting phenomena. In the following, the presented results were obtained with the stainless steel rods of different diameters. The

influence of both the contact length in each liquid and their height was experimentally verified too. The climbing height along the rod was independent of these parameters as long as the height of the oil phase exceeded the climbing value and the aqueous phase had a minimum height of 25 mm. For the sake of simplicity, all experiments presented below were carried out with a fixed height of 45 mm for each phase. The distance between the rod tip and the column bottom was also kept constant at 15 mm.

The visualization of the climbing phenomenon was realized by a high-speed digital camera Phantom v711 (Vision Research, USA) up to 1 million frames per second (fps). The typical acquisition rate was under 500 fps with a full resolution (1280×800). The image sequences obtained were then analyzed through Matlab. As long as the rotation speed wasn't too fast, the topology of the interface after the starting of the rod rotation reached quickly a stationary state with an axisymmetric shape, typically within 3 s. In the following, the reported results concern mainly the permanent regime except under very high rotation speeds. The light was provided by an indirect 800 W halogen which enlightened the column via indirect lighting on a white screen placed behind the column.

Instantaneous velocity fields around a rotating rod were measured using a Particle Image Velocimetry (PIV, Dantec Dynamics, Denmark) device shown in Figure 1. Illumination sheets were generated with two pulsed Nd:YAG lasers arranged side-by-side and crossed the vertical symmetry axis of the rod. Then, the half of the axisymmetric flow fields around the rod was determined. Both phases were inseminated with fluorescent polymer beads (Rhodamine B) of

15 μm as seeding particles. An orange filter placed in front of the camera eliminated the reflections of the lasers on the rod and let only the fluorescent light of the particles pass. The camera, placed perpendicular to the laser sheet, took two successive images, each at the maximum intensity of the laser impulse. These images were divided into a few thousands of small interrogation areas of 32×32 pixels. A cross-correlation was then performed on the two corresponding interrogation areas. This cross-correlation gave then the flow field in liquids around the rotating rod. The PIV device allowed also the determination of the velocity at different positions in the square, in particular, inside the heavy aqueous phase where the rod-climbing takes place.

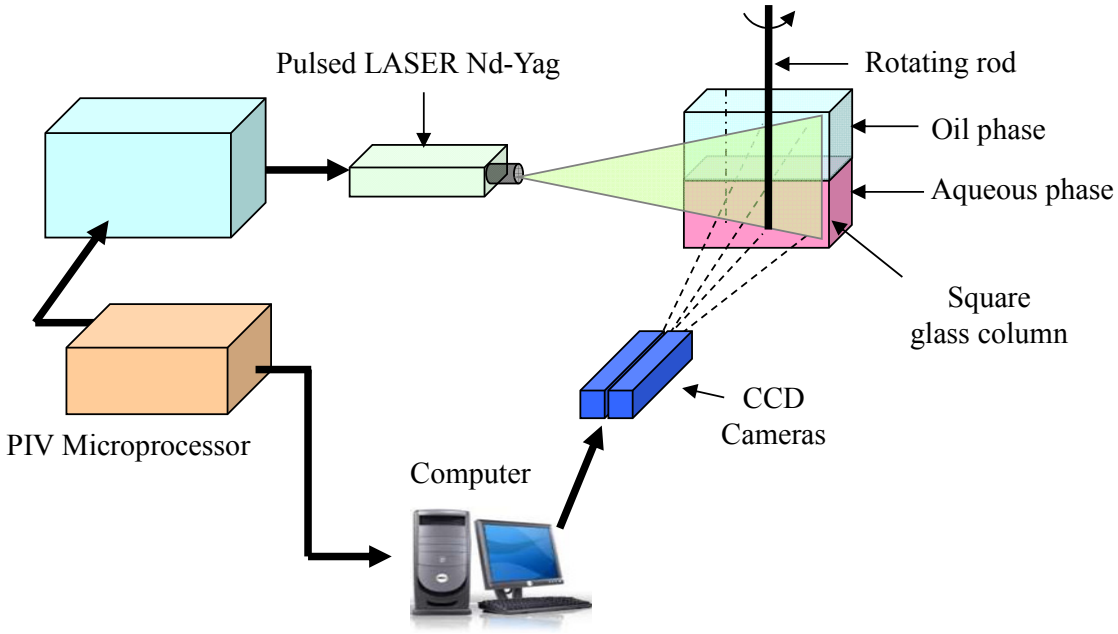

Figure 1. PIV experimental setup.

III. EXPERIMENTAL RESULTS

When the rotation speed was relatively low, the interface kept its flat topology without

observable modification. Beyond a certain value, the Weissenberg-like effect began to take place through the visual observation of the rod-climbing. A typical example is shown in Fig. 2 for the system composed of water and silicon oil of viscosity 111 mPa.s (SO111). However, an exact determination of a critical threshold wasn't easy by the experimental visualization due to the small climbing magnitude as well as the presence of the above-mentioned meniscus near the column wall. The climbing height of the aqueous phase increased with the augmentation of the rotation speed and the climbing shape remained stable and axisymmetric in time. When the rotation speed was too fast, the shape of climbing liquid became instable before forming ring structure and breaking up into water drops in the SO111 phase. It was then meaningless to determine a reliable climbing height above a rotation speed of 500 rpm in the case of a water-SO111 with a rod of 10 mm (e.g. Fig. 2a, $N = 600$ rpm).

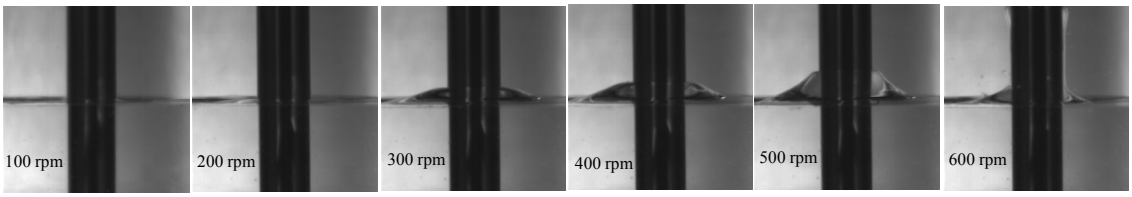

(a)

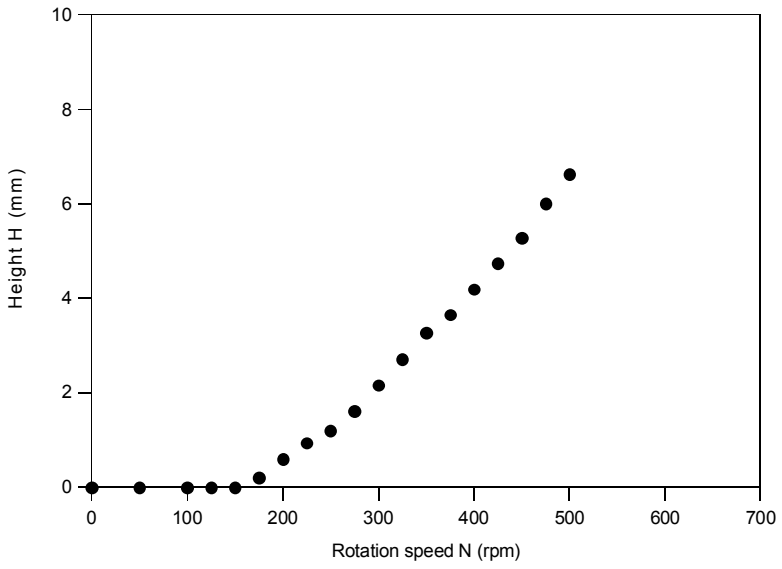

(b)

Figure 2. Weissenberg-like effect: climbing height H as a function of the rotation speed of the rod N for the interface composed of water - silicon oil 111 mPa.s (SO111), rod diameter d = 10 mm.

Our experiments highlight that the diameter of the rotation rod plays a main role in the climbing height. In Fig. 3a, an example is shown with the HV45 25% - SO111 with three different rod diameters. All other conditions being equal, a smaller rod required faster rotation to reach a same climbing height. A full dimensional analysis was performed to find a suitable scaling in terms of the relevant dimensionless numbers. But various attempts by means of the Reynolds number Re, Taylor number Ta and even Ekman number Ek proved futile. An example was illustrated in Fig. 3b between the normalized climbing height by the rod diameter H/d and the rotational Reynolds number with the properties of the aqueous phase $Re_A = Nd^2 / \upsilon_A$, as the climbing phase was the aqueous 25% HV45. The main difficulty in gathering data in a master curve seems to arise from the presence of two liquid phases instead

of a single component liquid phase.

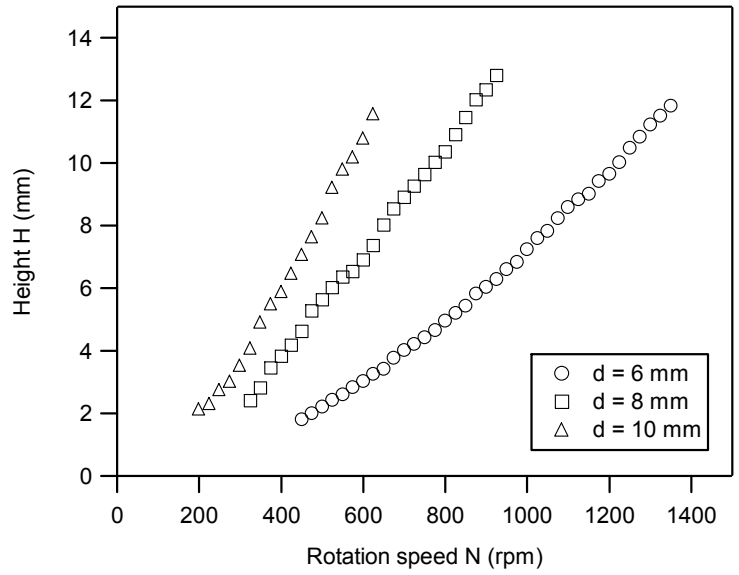

(a)

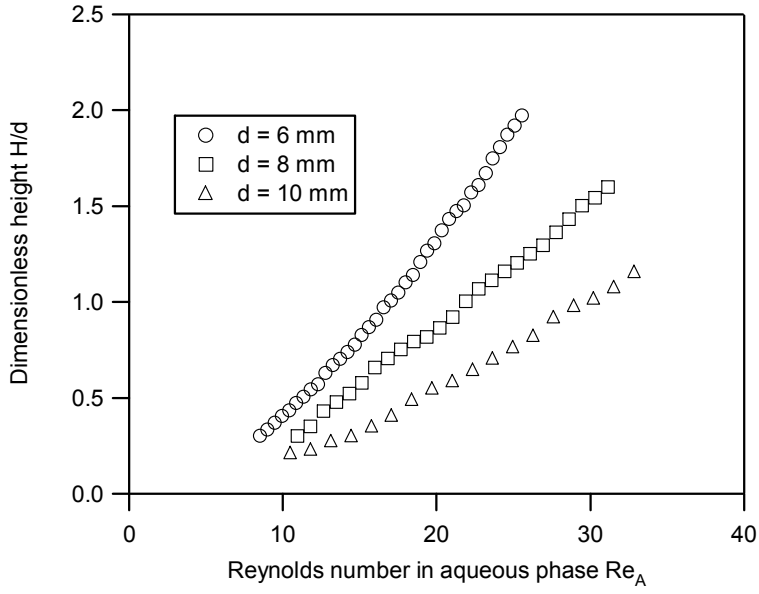

(b)

Figure 3. Interface composed of HV45 25% - SO111. (a) influence of the rod diameter on the climbing height *H*. (b) normalized climbing height *H*/*d vs*. rotation Reynolds number with

aqueous phase properties $\mathrm{Re}_A = Nd^2/\upsilon_A$.

Among various liquid-liquid interfaces investigated, an initially flat interface could also descend towards the column bottom, in a contrary direction to the climbing (Fig. 4a). A descending height was measured, and its magnitude increased with both the rotation speed and the diameter of the rod as for the climbing (Fig. 4b). A systematic scanning of the operating conditions revealed that the ratio of the kinematic viscosity between aqueous and oil phases was the unique parameter that determined the topological orientation of the interface. The interface exhibited the Weissenberg-like climbing effect when the heavy aqueous phase was less viscous than the light oil phase. On the contrary, the interface came down, and to some extent was quite similar to the formation of a vortex flow in water drainage with a deformed free surface. Certainly, a liquid-liquid interface is more complex than a water-air free surface. Fig. 5 shows the interface behavior with a heavy HV45 50% aqueous phase and three silicon oils of different viscosity: 111, 500 and 1000 mPa.s. The corresponding ratio of kinetic viscosity between aqueous and oil phases for these three systems was υ_A/υ_O = 1.89, 0.42 and 0.21 respectively. Clearly, the orientation of the interface was modulated by the ratio of the kinematic viscosity: $\upsilon_A/\upsilon_O < 1$ for Weissenberg-like rod-climbing and $\upsilon_A/\upsilon_O > 1$ for the interface descending. Some preliminary experiments with water/decane for $\upsilon_A/\upsilon_O = 1.09$ indicated qualitatively that the interface remained quite flat within the experimental accuracy. Due to the volatility of the decane, such experiments were quite delicate to perform in time. These observations begin to throw some qualitative insight into the Weissenberg-like effect in Newtonian fluids. Unlike the normal forces for the rod-climbing in a viscoelastic non-Newtonian fluid, the climbing or

descending effect should stem from a hydrodynamic mechanism. Under the continuous rotation of a rod, hydrodynamic effects should push the less viscous fluid to climb along the rod to enter in the more viscous one and result then in a consecutive topology of interface.

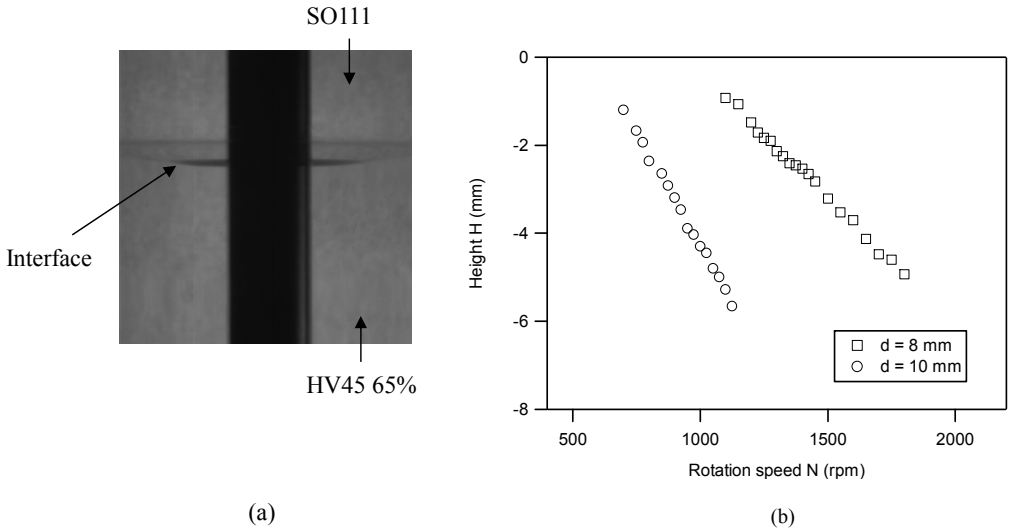

Figure 4. Descending phenomena with the interface composed of HV45 65% - SO111. (a) descending interface with d = 10 mm and N = 900 rpm. (b) influence of the rotation speed N on the descending height H.

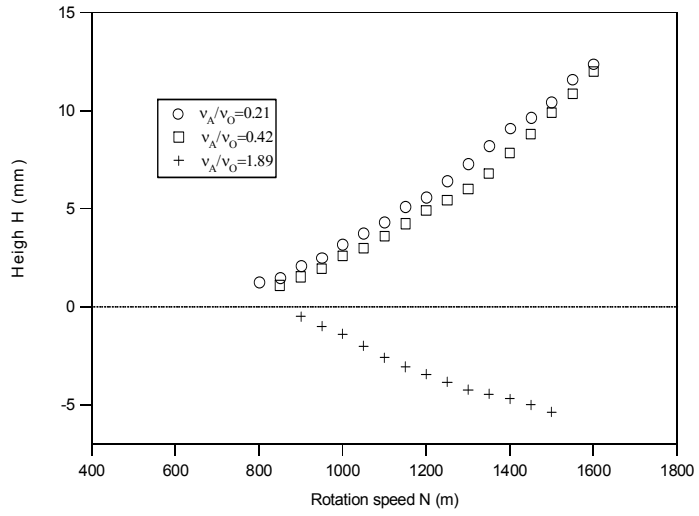

Figure 5. Interface orientation as a function of the ratio of kinematic viscosity between two

phases. Interfaces: aqueous phase HV45 50%; oil phases SO111, SO500 and SO1000 respectively, rod diameter d = 10 mm.

These intuitions were corroborated by the PIV measurements of flow fields. A flow field near the interface composed of water and silicon oil 111 mPa.s is illustrated in Fig. 6. Clearly, the flow in the more viscous SO111 is mainly azimuthal in a quasi-laminar regime; on the other hand, the less viscous water exhibits a strong ascension near the rod that is certainly the driving force of the observed Weissenberg-like effect. The camera in the PIV technique having a limited windows of the observation, the square tank was already too large to ensure simultaneously the measurements of complete flow fields in each phase. To gain better understanding in the climbing phase, PIV measurements were then focused on the climbing aqueous phase. The complete flow field inside the less viscous aqueous phase is shown in Fig. 7 under different rotation speeds. The appearance of a flow instability in the form of toroidal Taylor-Couette vortices could be responsible for the Weissenberg-like effect, even if the liquids were not spatially confined in this work as in a classical Taylor-Couette device. Two immiscible liquids being simultaneously present in the column, increasing the rotation speed of the rod undergoes a progression of the size of such vortices whose center displaces towards the column wall. The amplification of the Taylor-Couette vortices due to the more energy dissipation contributes to the augmentation of the climbing height. These PIV results concerning the flow fields seem to confirm the modulation mechanism of the interface's topology: a dynamical competition for the early appearance of the Taylor-Couette vortices according to the ratio of the kinematic viscosity between two Newtonian phases υ_A / υ_O.

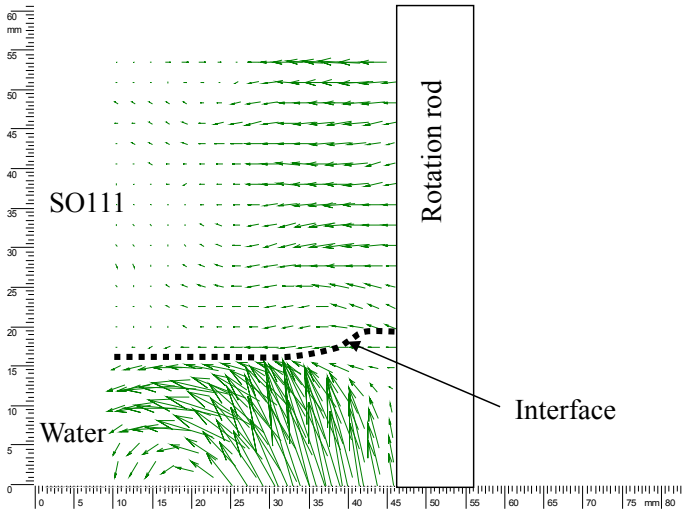

Figure 6. Flow fields measured by the PIV device in both phases with the interface water – SO111, d = 10 mm and N = 400 rpm.

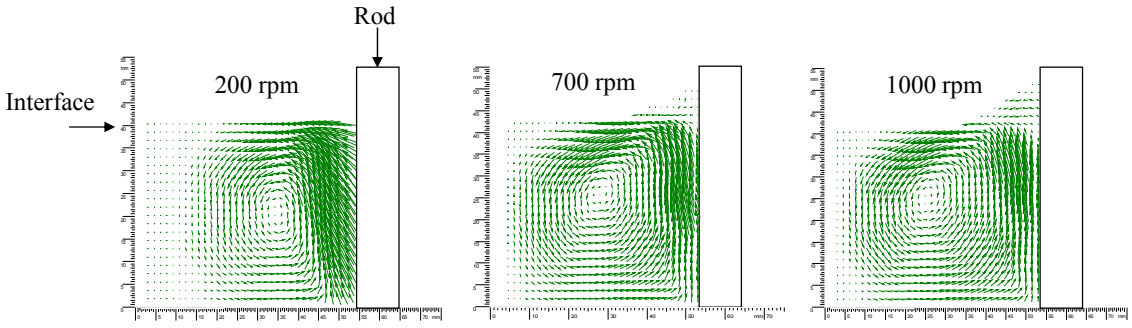

Figure 7. Flow fields measured by the PIV device in the climbing aqueous phase under different rotation speeds. Interface composed of HV45 25% - SO111, rod diameter d = 10 mm.

IV. NUMERICAL SIMULATION WITH VOLUME OF FLUID (VOF) APPROACH

A numerical approach based on the VOF method[16] was employed to simulate the flow pattern, in particular the interface position between two immiscible fluids within the framework of the commercial code Fluent 6.3. The VOF approach is a surface tracking technique applied to a fixed Eulerian mesh. The fields for all variables and properties are shared by the phases and represent volume-averaged values.

In this work, the tracking of the interface was performed by solving the transport equation for the aqueous phase volume fraction α_A varying between 0 and 1:

$$\frac{\partial \alpha_A}{\partial t} + \mathbf{u} \cdot \nabla \alpha_A = 0 \qquad (1)$$

A single set of Navier-Stokes equations was solved for the mixture of both fluids:

$$\frac{\partial \rho}{\partial t} + \nabla \cdot (\rho \mathbf{u}) = 0 \qquad (2)$$

$$\frac{\partial}{\partial \mathrm{t}} (\rho \mathbf{u}) + \nabla \cdot (\rho \mathbf{u}\mathbf{u}) = -\nabla p + \rho \mathbf{g} + \nabla . \left[\mu \left(\nabla \mathbf{u} + \nabla \mathbf{u}^T \right) \right] + \mathbf{F}_\sigma \qquad (3)$$

These two equations depend on the volume fractions through the characteristics of the density and viscosity. These properties were determined by the presence of the phases in each computational cell:

$$\rho = \alpha_A \rho_A + (1 - \alpha_A) \rho_O \qquad (4)$$

$$\mu = \alpha_A \mu_A + (1 - \alpha_A) \mu_O \qquad (5)$$

The term $\mathbf{F}_\sigma$ in the momentum equation is a surface tension source term, estimated using the continuum surface model of Brackbill *et al.*[17]. The interface unit normal was calculated by:

$$\mathbf{n} = \frac{\nabla \alpha_A}{|\nabla \alpha_A|} \qquad (6)$$

and the surface curvature as:

$$\kappa = -\left(\nabla.\mathbf{n}\right) \tag{7}$$

Then the surface tension source term was obtained by the following expression:

$$\mathbf{F}_{\sigma} = \sigma\kappa\nabla\alpha_{A}\frac{2\rho}{\rho_{O}+\rho_{A}} \tag{8}$$

The Youngs' piecewise linear interface construction (PLIC) scheme[18] was used to reconstruct the interface in the cells where $0 < \alpha_A < 1$. σ is the interfacial tension between two liquids. Transient computations were performed and the pressure-implicit with splitting of operators (PISO) scheme was employed for the pressure-velocity coupling treatment.

Due to the complex nature of the Weissenberg-like effect revealed by the PIV measurements, a 3D simulation was carried out. The top and bottom boundary conditions employed here were free surface and wall. Several mesh sizes were tested and a compromise was chosen between the computational accuracy and time. The column volume was meshed using a structured hexahedral mesh (435 000 cells). The mesh was particularly refined around both the rotating rod and the deformed liquid-liquid interface: cells of around $0.2\times0.2\times0.2$ mm^3 were used at the rod surface and near the interface, and their size grew progressively to reach $2\times2\times2$ mm^3 near the column walls.

Before starting the computation, an initial state was chosen with a flat interface between the two fluids that remain at rest. Calculations were performed with a time step of 1 ms until to reach a stationary shape of the interface. The rod was modelled as a wall with an angular velocity. No slip boundary conditions were applied to the column walls.

A typical numerical result is shown in Fig. 8 for the interface composed of water-SO111. The simulated climbing effect and the shape of the interface compare favorably with the experimental observation. The influence of the rotation speed of the rod on the climbing height is also clearly demonstrated in Fig. 9, although the VOF approach overestimates somewhat the value with respect to the experiments. Table III illustrates the outcome of such a comparison. The deviation could be attributed to both the experimental inaccuracy and numerical imprecision.

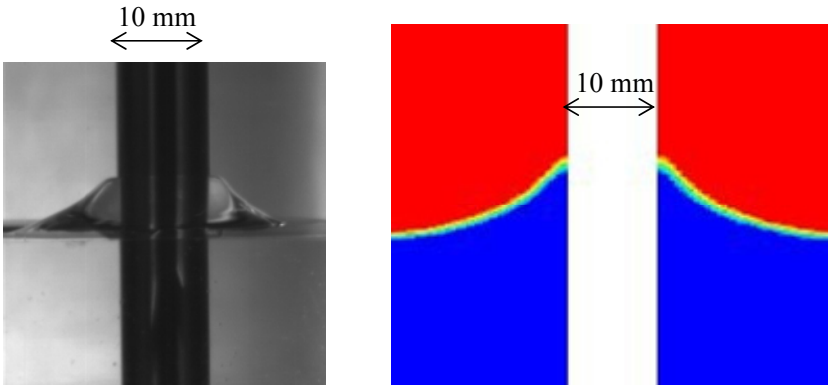

Figure 8. Comparison of the experimental (left) and simulated (right) climbing height for the interface water - SO111, rod diameter d = 10 mm and N = 500 rpm.

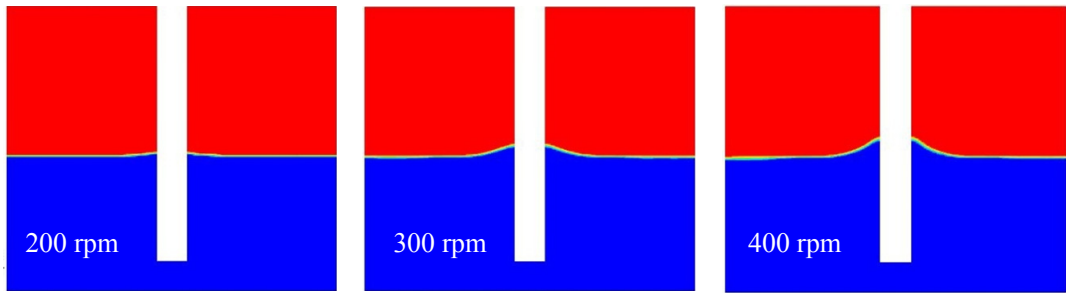

Figure 9. Simulated influence of the rotation speed of the rod N on the climbing height H for the interface water - SO111, rod diameter d = 10 mm by VOF.

Moreover, it is worth noting that the experimentally observed climbing instability under high rotation speeds of the rod is numerically reproduced by the VOF approach as shown in Fig. 10. The main instability features in the form of rings along the rod are qualitatively captured by the simulation in spite of a certain difference in the exact value of the rotation speed of the rod. In fact, a destabilization of the interface occurs for $N \geq 650$ rpm, this threshold is a higher than the experimental one that is about 530 rpm. It is worth noting that the scale shown Fig. 10 is different between the numerical and experimental results. When the instability occurs, the interface oscillates with time and is no longer axisymmetric compared to the case under smaller rotation speeds. The simulation could not go further when the climbing instability appeared as a singular event to induce difficulties in numerical convergence regardless of refined mesh sizes. Experimentally, the appearance of the secondary instability is usually accompanied by the formation of ring structures climbing much higher along the rod. These rings can breakup into small water drops in the oil phase with the increase of the rotation speed of the rod. The VOF approach can qualitatively describe these experimental observations, but fails in producing quantitatively satisfactory agreement with the experimental data. This deviation would mainly stem from the lack of physical knowledge involved in the commercial software, for example complex wetting dynamics between rod and liquid-liquid interfaces.

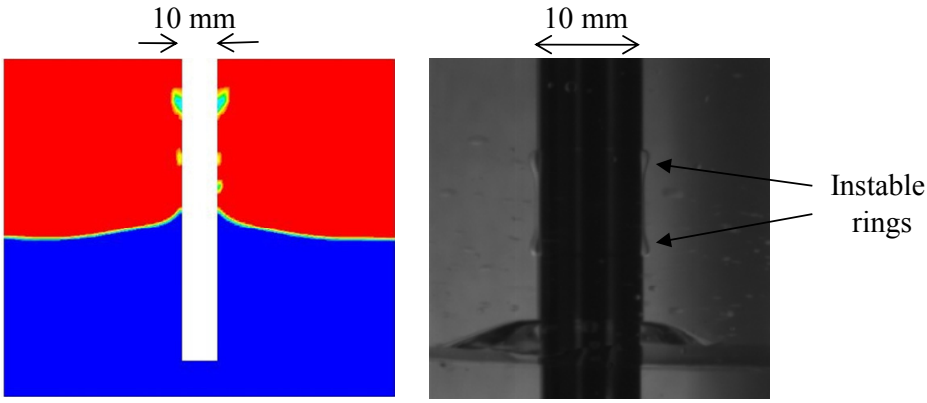

Figure 10. Climbing instability under high rotation speeds for the interface water – SO111. (a) VOF simulation, N = 700 rpm. (b) Experimental, N = 630 rpm.

V. CONCLUSION

The dynamical modulation by a rotating rod of a liquid-liquid interface composed of both Newtonian liquids was addressed in the present work. Major operating parameters such as the rotation speed of the rod, rod diameter and especially various liquid-liquid interfaces were experimentally investigated by the camera visualization and the PIV technique. The direct visualization of the interface's topology reveals that the ratio of kinematic viscosity between the aqueous and oil phases seems to be the key parameter for the orientation of the interface: $\upsilon_A / \upsilon_O < 1$ for the Weissenberg-like rod-climbing and $\upsilon_A / \upsilon_O > 1$ for the interface descending. The measurements of the flow fields in both phases, in particular within the aqueous phase in the case of rod-climbing, established a relationship between the interface orientation and the first appearance of the Taylor-Couette vortices in the less viscous phase. The continuous rod rotation maintains these vortices in a permanent way so that the climbing

is a stationary and axisymmetric phenomenon as long as the rotation speed doesn't exceeds a certain limit. The intensity of this instability increases with the rotation speed of the rod, and then amplifies the climbing height. However, very high rotation speeds of the rod lead to secondary instabilities, causing especially the breakup of the climbing liquid and the dissymmetric climbing interface.

The numerical simulation by the VOF approach can reproduce to some extent the rod-climbing or rod-descending effects. The simulated interface climbing is in agreement with the experimental observation. Besides, the influence of the rotation speed on the climbing height is predicted compared to the experiments. Although the VOF simulation could describes qualitatively the above-mentioned phenomena, including dissymmetric climbing interfaces along the rod under high rotation speeds. , the quantitative agreement is partially satisfactory for such as the climbing height and in particular secondary instabilities in the climbing liquid with the ring formation and breakup under high rotation speeds of rod. It is worth mentioning that further both experimental and numerical efforts are still required to better understand these complex dynamical phenomena at liquid-liquid interface which play a central role in numerous industrial processes involving liquid-liquid dispersions such as emulsification. In addition to investigations by commercial software, a more reliable physical modelling[19] taking into account local interfacial behavior such as triple line contact dynamics at the rod surface would be essential.

ACKNOWLEDGMENTS

The financial support provided by the French Ministère de l'Enseignement Supérieur et de la Recherche and the CNRS is gratefully acknowledged.

References

1. G. G. Fuller and J. Vermant, "Editorial: dynamics and rheology of complex fluid–fluid interfaces," Soft Matter 7, 7583-7585 (2011).

2. R. J. Stokes and D. Fennell Evans, *Fundamentals of Interfacial Engineering*, Wiley-VCH, New York (1997).

3. Z. Mohamed-Kassim, E. K. Longmir, "Drop impact on a liquid/liquid interface," Phys. Fluids 15, 3263-3273 (2003).

4. X. P. Chen, S. Mandre, J. J. Feng, "Partial coalescence between a drop and a liquid-liquid interface," Phys. Fluids 18, 051705 (2006).

5. S. Hartland, "The approach of a rigid sphere to a deformable liquid/liquid interface," J. Colloid Interface Sci. 26, 383-394 (1968).

6. N. Dietrich, S. Poncin and H. Z. Li, "Passage of a settling sphere through a liquid-liquid interface,"Exp. in Fluids 50, 1293-1303 (2011).

7. A. F. Jones, S. D. R. Wilson, "The film drainage problem in droplet coalescence," J. Fluid Mech. 87, 263-288 (1978).

8. Z. Mohamed-Kassim, E. K. Longmir, "Drop coalescence through a liquid/liquid interface," Phys. Fluids 16, 2170-2181 (2004).

9. R. Bonhomme, J. Magnaudet, F. Duval B. Piar, "Inertial dynamics of air bubbles crossing a

horizontal fluid-fluid interface," J. Fluid Mech. 707, 405-443 (2012).

10. N. Dietrich, S. Poncin, S. Pheulpin and H. Z. Li, "Bubble passage at a liquid-liquid interface," AIChE J. 54, 594-600 (2008).

11. A. S. Geller, S. H. Lee and L. G. Leal, "The creeping motion of a spherical particle normal to a deformable interface," J. Fluid Mech. 169, 27-69 (1986).

12. D. Bonn, M. Kobylko, S. Bohn, J. Meunier, A. Morozov and W. van Saarloos, "Rod-climbing effect in Newtonian fluids," Phys. Rev. Lett. 93, 214503 (2004).

13. K. Weissenberg, "A continuum theory of rheological phenomena," Nature, 159, 310-311 (1947).

14. G. I. Taylor, "Stability of a viscous liquid contained between two rotating cylinders," Phil. Trans. R. Soc. London A 223, 289-343 (1923).

15. R. J. Stokes and D. F. Evans, in *Fundamentals of interfacial engineering*, Wiley-VCH New York (1997)

16. C. W. Hirt and B. D. Nichols, "Volume of fluid for the dynamics of free boundaries," J. Comput. Phys. 39, 201-255 (1981).

17. J. U. Brackbill, D. B. Kothe and C. Zemach, "A continuum method for modeling surface tension," J. Comput. Phys. 100, 335-354 (1992).

18. D. L. Youngs, in *Numerical methods for fluid dynamics*, ed. K. W. Morton, M. J. Baines, Academic Press, New York (1982).

19. X. Frank and H. Z. Li, "Negative wake behind a sphere rising in viscoelastic fluids: a lattice Boltzmann investigation," Phys. Rev. E 74, 056307 (2006).

Caption of tables

Table I. Physical properties of different liquids used in this study at 293K.

Table II. Interfacial tension of different liquid-liquid systems at 293K.

Table III. Comparison of the increasing climbing height with the rotation speed between the VOF simulation and experimental observation for water-SO111. Rod diameter d = 10 mm.

Caption of figures

Figure 1. PIV experimental setup.

Figure 2. Weissenberg-like effect: climbing height H as a function of the rotation speed of the rod N for the interface composed of water - silicon oil 111 mPa.s (SO111), rod diameter d = 10 mm.

Figure 3. Interface composed of HV45 25% - SO111. (a) influence of the rod diameter on the climbing height H. (b) normalized climbing height H/d *vs*. rotation Reynolds number with aqueous phase properties $\mathrm{Re}_A = Nd^2 / \upsilon_A$.

Figure 4. Descending phenomena with the interface composed of HV45 65% - SO111. (a) descending interface with d = 10 mm and N = 900 rpm. (b) influence of the rotation speed N on the descending height H.

Figure 5. Interface orientation as a function of the ratio of kinematic viscosity between two

phases. Interfaces: aqueous phase HV45 50%; oil phases SO111, SO500 and SO1000 respectively, rod diameter d = 10 mm.

Figure 6. Flow fields measured by the PIV device in both phases with the interface water – SO111, d = 10 mm and N = 400 rpm.

Figure 7. Flow fields measured by the PIV device in the climbing aqueous phase under different rotation speeds. Interface composed of HV45 25% - SO111, rod diameter d = 10 mm.

Figure 8. Comparison of the experimental (left) and simulated (right) climbing height for the interface water - SO111, rod diameter d = 10 mm and N = 500 rpm.

Figure 9. Simulated influence of the rotation speed of the rod N on the climbing height H for the interface water - SO111, rod diameter d = 10 mm by VOF.

Figure 10. Climbing instability under high rotation speeds for the interface water – SO111. (a) VOF simulation, N = 700 rpm. (b) Experimental, N = 630 rpm.

Table I. Physical properties of different fluids used in this study at 293 K.

	Water	HV45 25%	HV45 50%	HV45 65%	SO11	SO111	SO500	SO1000
Density ρ ($kg.m^{-3}$)	996	1010	1030	1050	920	960	961	970
Viscosity $\mu \times 10^3$ (Pa.s)	1	32	225	665	11	111	500	1000
Kinematic viscosity $\upsilon \times 10^6$ ($m^2.s^{-1}$)	1.0	29.7	218.4	633.3	12.0	115.6	520.3	1030.9

Table II. Interfacial tension of different liquid-liquid systems at 293 K.

Interfacial tension $\sigma \times 10^3$ ($N.m^{-1}$)	SO11	SO111	SO500	SO1000
Water	22.2	17.6	17.1	17.0
HV45 25%	18.2	16.9	16.9	16.8
HV45 50%	15.2	15.5	15.4	15.5
HV45 65%	14.9	15.1	15.2	15.1

Table III. Comparison of the increasing climbing height with the rotation speed between the VOF simulation with an uncertainty of 3% and experimental observation with a uncertainty of 5% for water-SO111. Rod diameter d = 10 mm.

Climbing height H (mm)	N = 200 rpm	N = 300 rpm	N = 400 rpm	N = 500 rpm
VOF simulation	1.20 ± 0.04	3.60 ± 0.11	5.80 ± 0.17	8.30 ± 0.25
Experimental observation	0.60 ± 0.03	2.20 ± 0.11	4.20 ± 0.21	6.60 ± 0.33

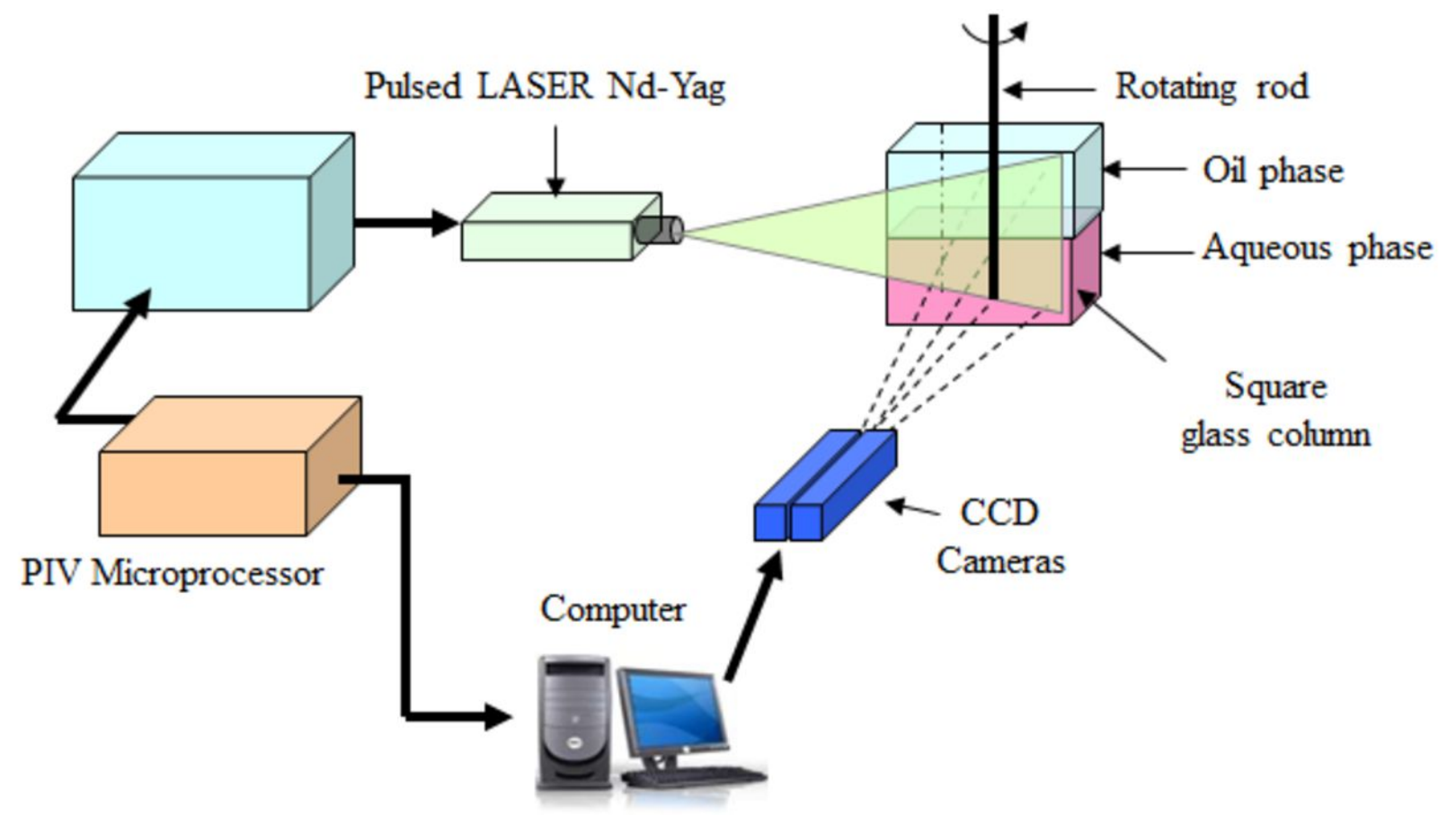
Pulsed LASER Nd-Yag
Rotating rod
Oil phase
Aqueous phase
Square
glass column
CCD
Cameras
PIV Microprocessor
Computer

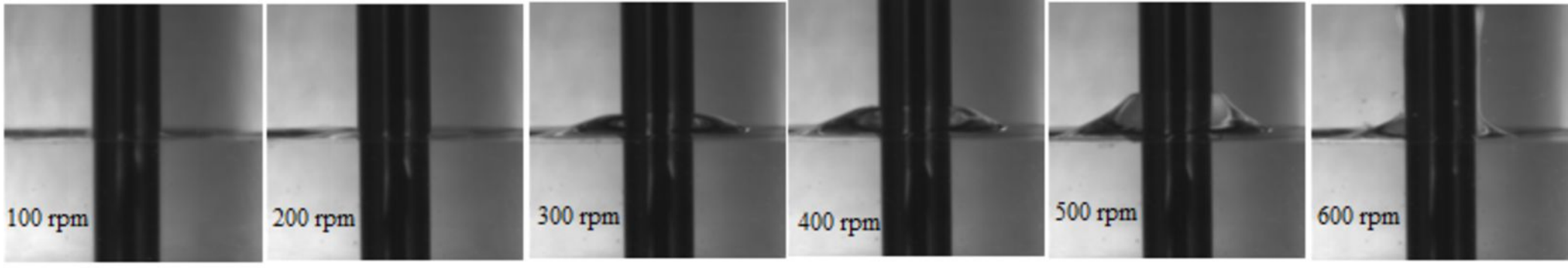
100 rpm
200 rpm
300 rpm
400 rpm
500 rpm
600 rpm

(a)

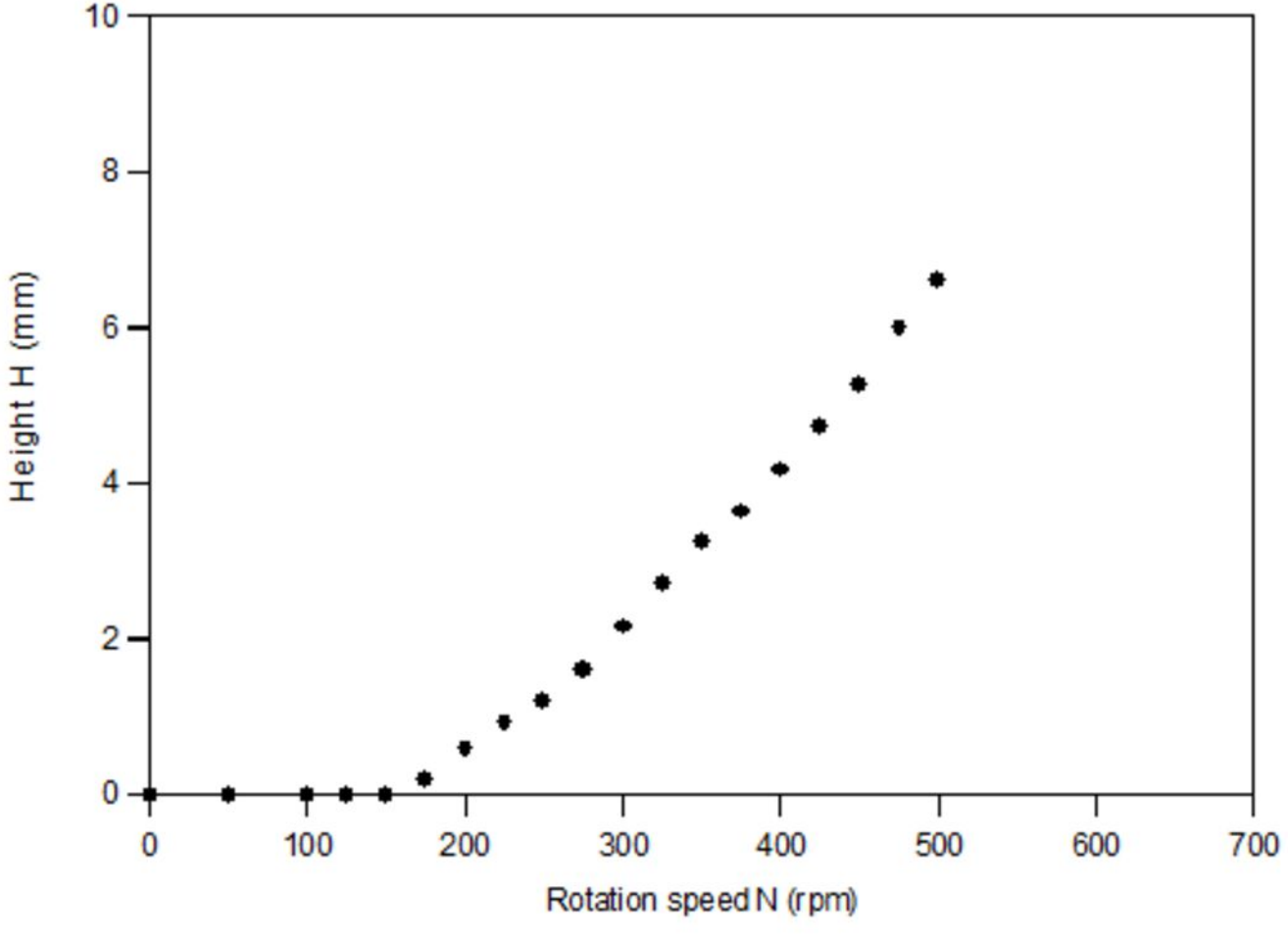
Height H (mm)
Rotation speed N (rpm)
0
2
4
6
8
10
0
100
200
300
400
500
600
700

(b)

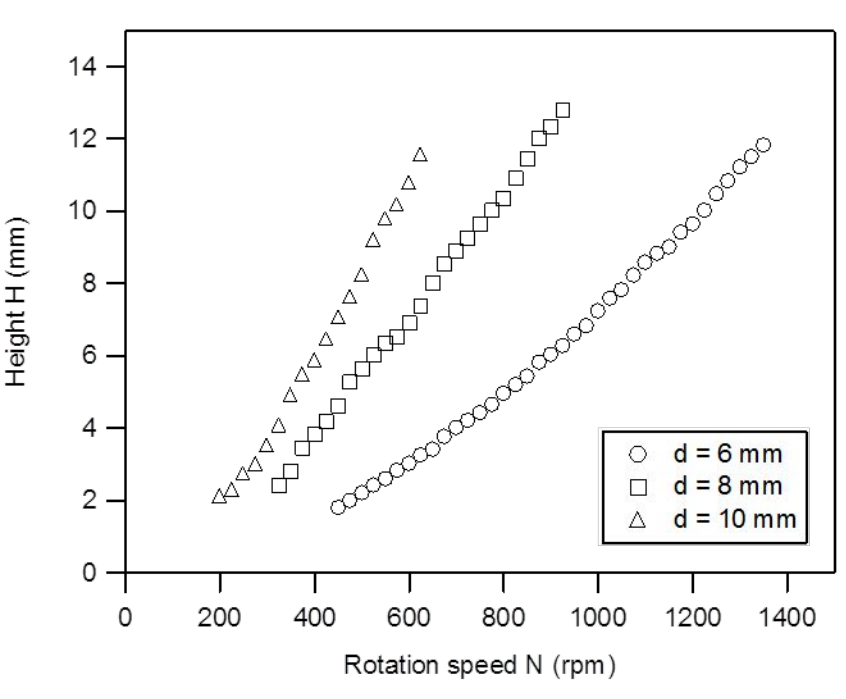
Height H (mm)
Rotation speed N (rpm)
d = 6 mm
d = 8 mm
d = 10 mm
0
2
4
6
8
10
12
14
0
200
400
600
800
1000
1200
1400

(a)

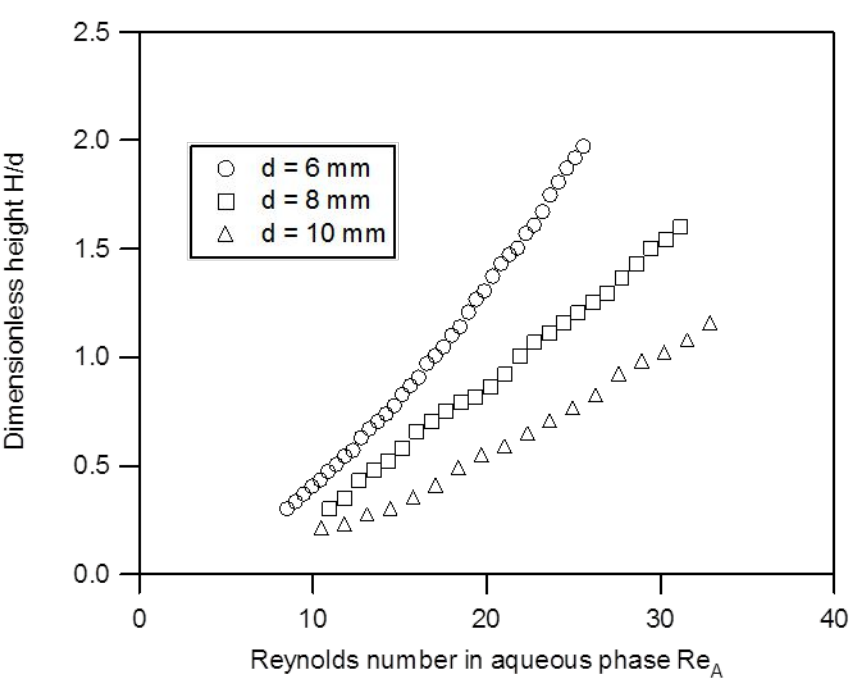
Dimensionless height H/d
Reynolds number in aqueous phase Re$_A$
d = 6 mm
d = 8 mm
d = 10 mm
0.0
0.5
1.0
1.5
2.0
2.5
0
10
20
30
40

(b)

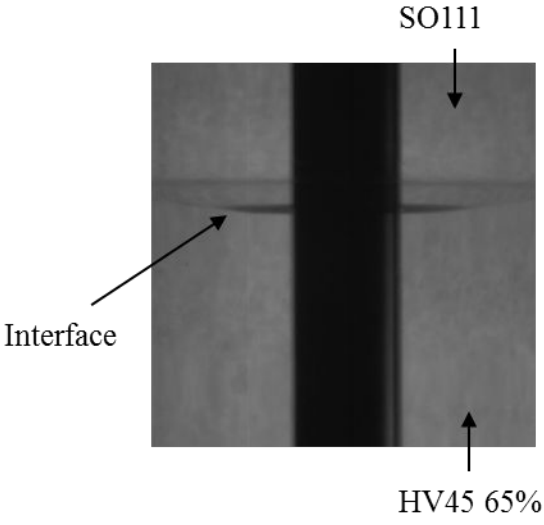
SO111
Interface
HV45 65%

(a)

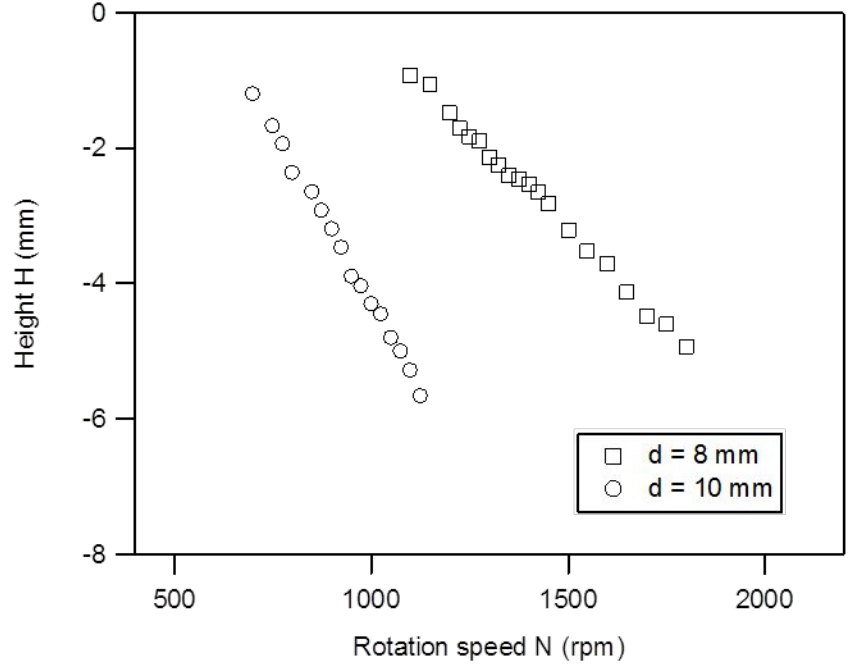
Height H (mm)
0
-2
-4
-6
-8
500
1000
1500
2000
Rotation speed N (rpm)
d = 8 mm
d = 10 mm

(b)

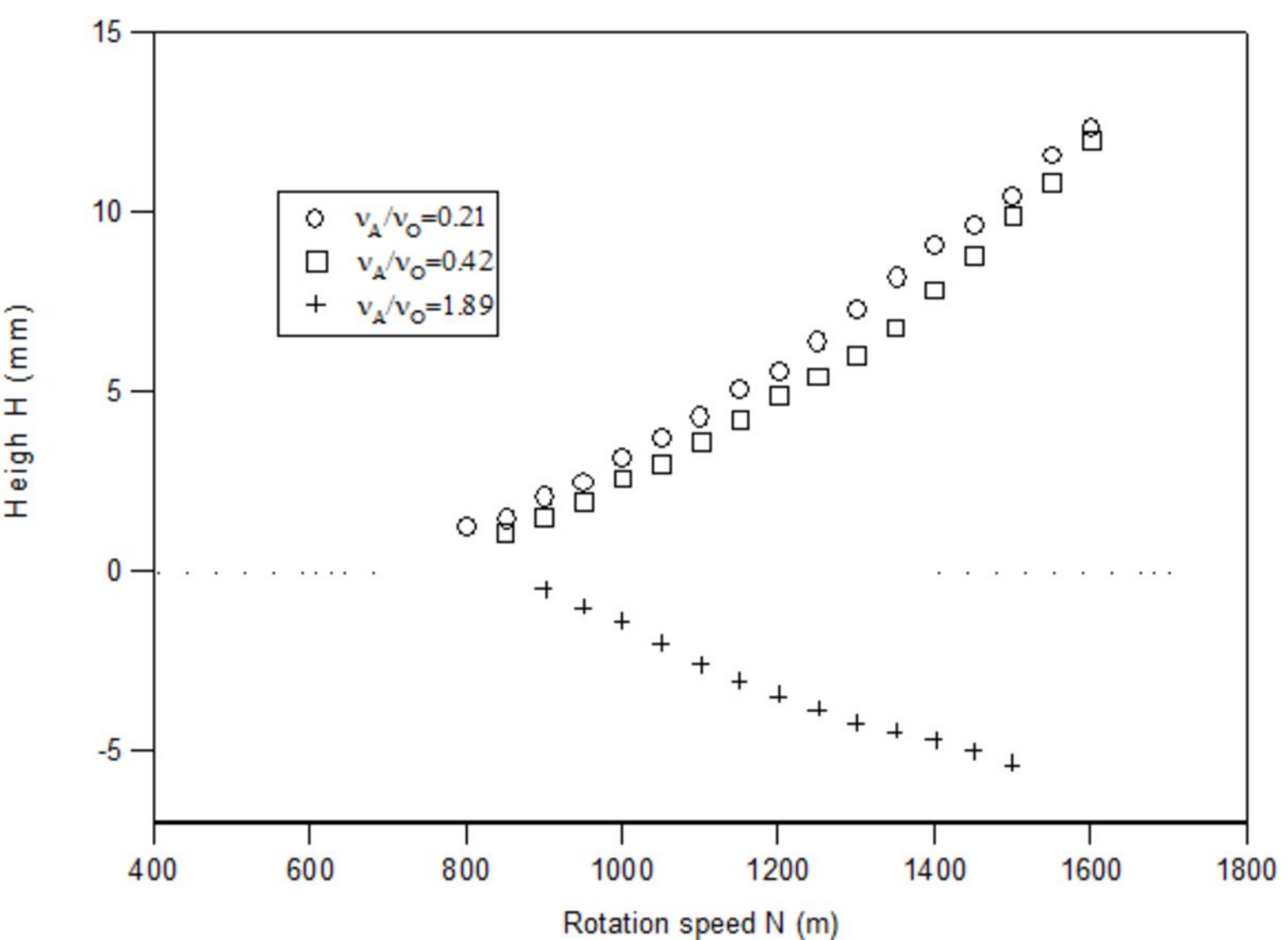
15
10
5
0
-5
Heigh H (mm)
ν_A/ν_O=0.21
ν_A/ν_O=0.42
ν_A/ν_O=1.89
400
600
800
1000
1200
1400
1600
1800
Rotation speed N (m)

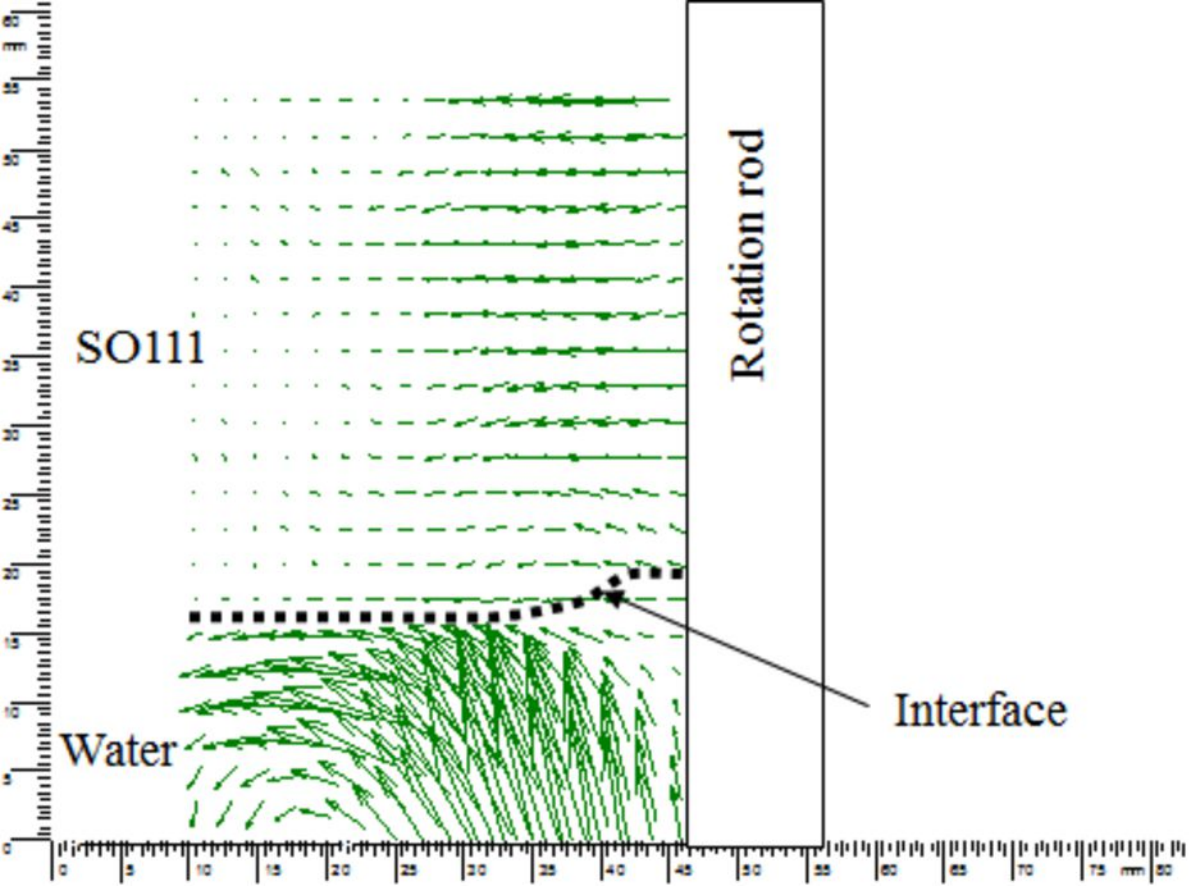
SO111
Rotation rod
Interface
Water

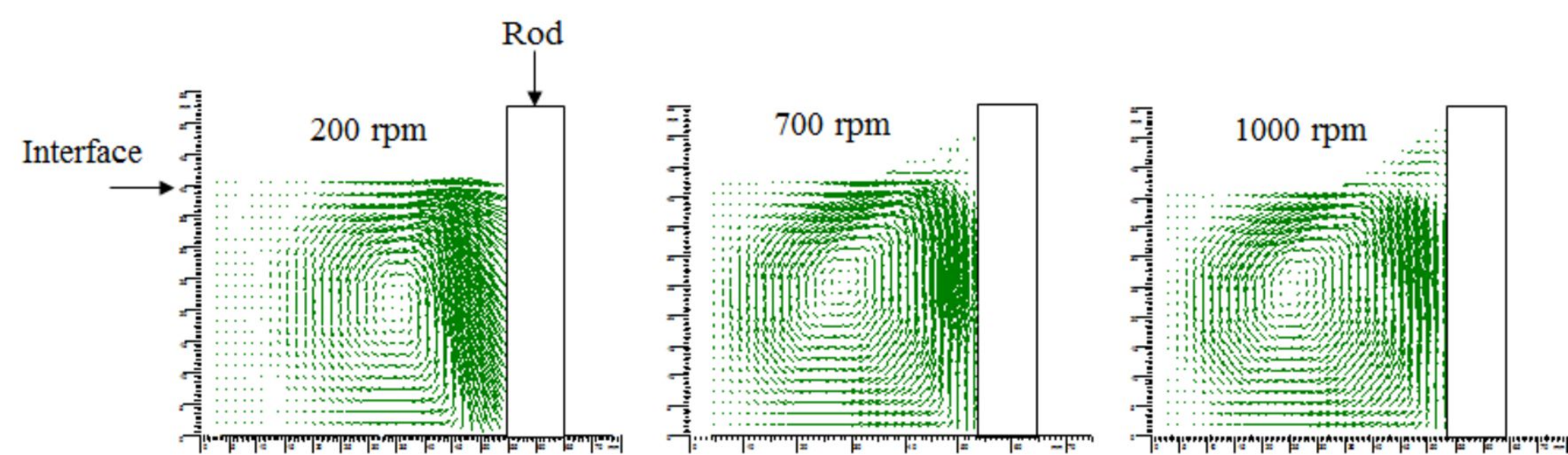
Rod
Interface
200 rpm
700 rpm
1000 rpm

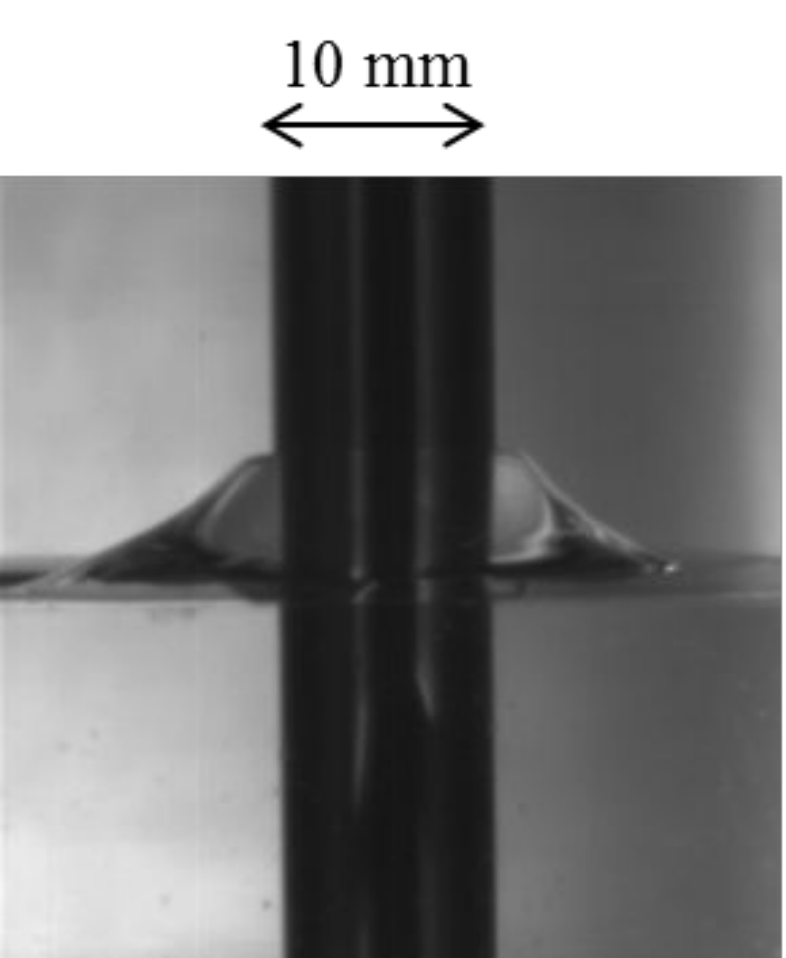
10 mm

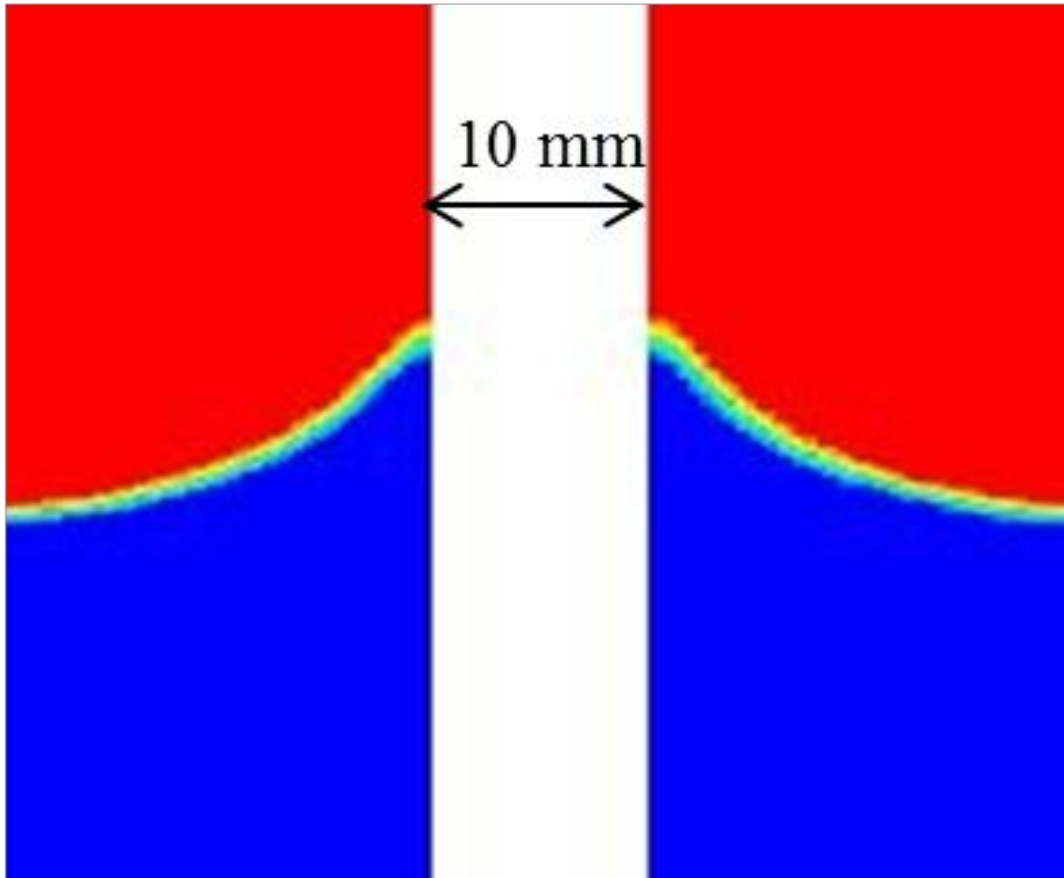
10 mm

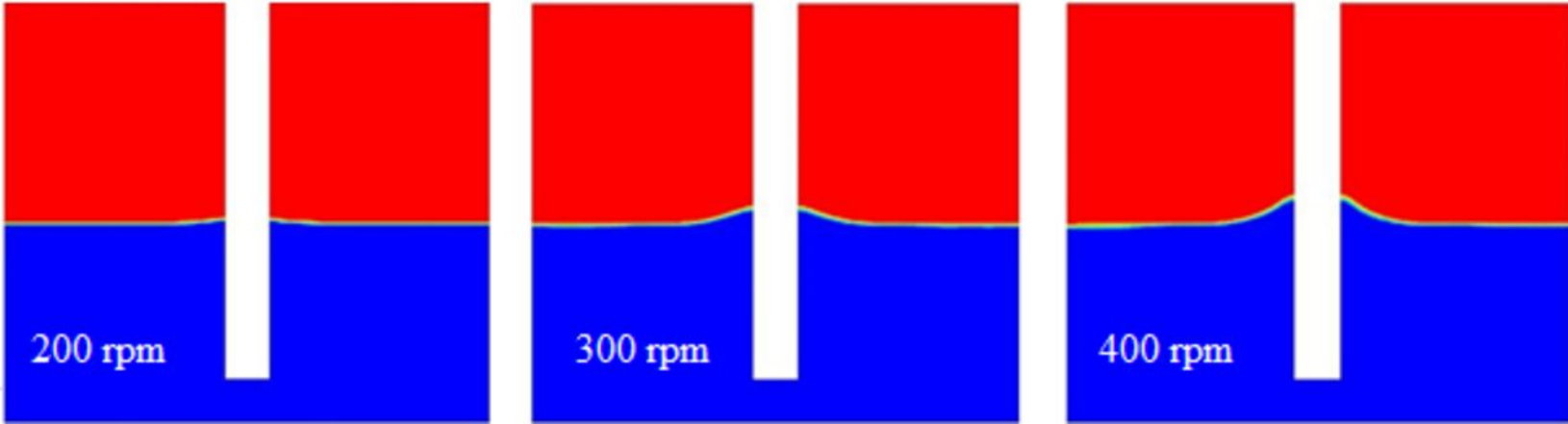
200 rpm
300 rpm
400 rpm

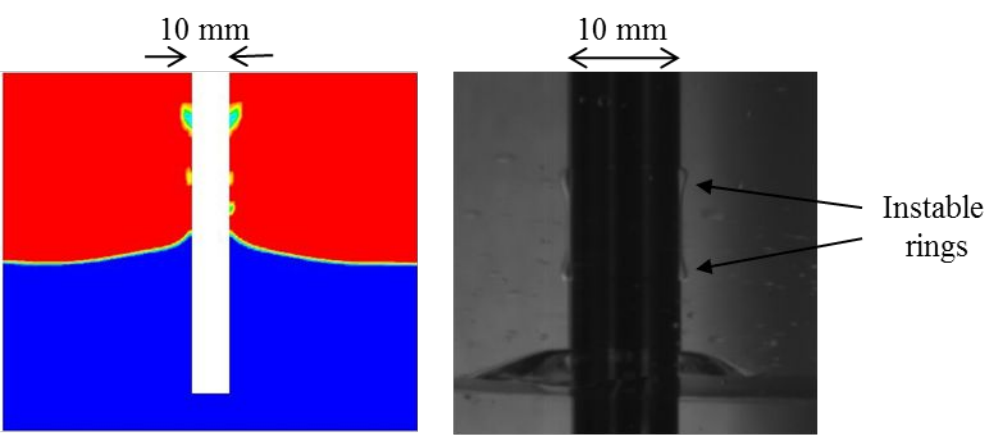
10 mm
10 mm
Instable
rings
(a)
(b)